

DIAGNOSTICS OF ATMOSPHERIC PRESSURE AIR PLASMAS

C.O. Laux^{*}, C.H. Kruger, and R.N. Zare^{**}

Thermosciences Division, Mechanical Engineering Department, Stanford University, Stanford, CA 94305, USA

Abstract — Atmospheric pressure air plasmas are often thought to be in Local Thermodynamics Equilibrium (LTE) owing to fast interspecies collisional exchanges at high pressure. As will be seen here, this assumption cannot be relied upon, particularly with respect to optical diagnostics. Large velocity gradients in flowing plasmas and/or elevated electron temperatures created by electrical discharges can result in large departures from chemical and thermal equilibrium. Diagnostic techniques based on optical emission spectroscopy (OES) and Cavity Ring-Down Spectroscopy (CRDS) have been developed and applied at Stanford University to the investigation of atmospheric pressure plasmas under conditions ranging from thermal and chemical equilibrium to thermochemical nonequilibrium. This article presents a review of selected temperature and species concentration measurement techniques useful for the study of air and nitrogen plasmas.

1 Introduction

The various techniques described in this article were applied to measurements in three types of air or nitrogen plasmas. The first case corresponds to an LTE air plasma produced by a 50 kW inductively coupled plasma torch, and flowing at a relatively low velocity of 10 m/s [1]. As the convective rates are slower than chemistry rates, and as the measurements are made in the field free region downstream of the induction coils, the plasma conditions approach LTE. The second case corresponds to recombining air or nitrogen plasmas, produced by the torch and flowed at high velocities approaching 1 km/s through a water cooled test section [2]. At these velocities, the convective rates are faster than the chemistry rates and the plasma reaches chemical nonequilibrium at the test-section exit owing to finite chemical recombination rates. However, as no electric field is applied in these experiments, the temperatures of free-electrons and heavy species are equilibrated and the flow is close to thermal equilibrium. The third case corresponds to atmospheric pressure glow discharges generated by a DC electric field in air or nitrogen [3, 4]. A characteristic of glow discharges is that the electron temperature T_e is elevated with respect to the gas temperature T_g of heavy species. Representative conditions are $T_e = 1$ eV and $T_g = 2000$ K. Under these conditions, energetic electrons cause a significant amount of dissociation and ionization. These plasmas are therefore in thermal and chemical nonequilibrium.

In all three cases, it can be assumed that the rotational temperature is close to the gas temperature owing to fast rotational relaxation at atmospheric pressure. On the other hand, no simple assumption holds regarding the vibrational and electronic population distributions. The often-used assumption that $T_{\text{electronic}}$ and $T_{\text{vibrational}}$ are approximately equal to the electron temperature is often invalid in nonequilibrium plasmas. Thus great care must be exercised in interpreting optical diagnostics in these flows. Section 2 of this article presents an overview of our experimental plasma generation and optical diagnostic facilities. Section 3 describes the spectroscopic model employed in our data analyses. Section 4 illustrates three methods for measuring the rotational temperature in air and nitrogen. Section 5 presents optical techniques for the determination of species concentrations including nitrogen and oxygen atoms, electrons, and charged species.

2. Experimental facilities

The air and nitrogen plasmas investigated in our laboratory are produced with a 50 kW inductively-coupled plasma torch operating at 4 MHz. The atmospheric pressure plasmas exit the torch through interchangeable nozzles with diameters from 1 to 7 cm. Figure 1a shows the torch head and plasma plume for our experiments with slow flowing, LTE air plasmas. Here the nozzle diameter is 7 cm. Faster flows are produced with smaller exit nozzle diameters. Figure 1b shows the experimental set-up for our recombination studies with air and nitrogen plasmas. In these studies, the exit nozzle diameter is 1 cm, and water cooled test-sections of various lengths are placed downstream of the torch in order to force fast plasma recombination in a well-controlled

^{*} Author to whom correspondence should be addressed

^{**} Chemistry Department, Stanford University

environment. Finally, Figure 1c shows the photograph of a glow discharge created by applying a DC electric field in a fast flowing (~ 450 m/s) low temperature (2200 K) atmospheric pressure air plasma.

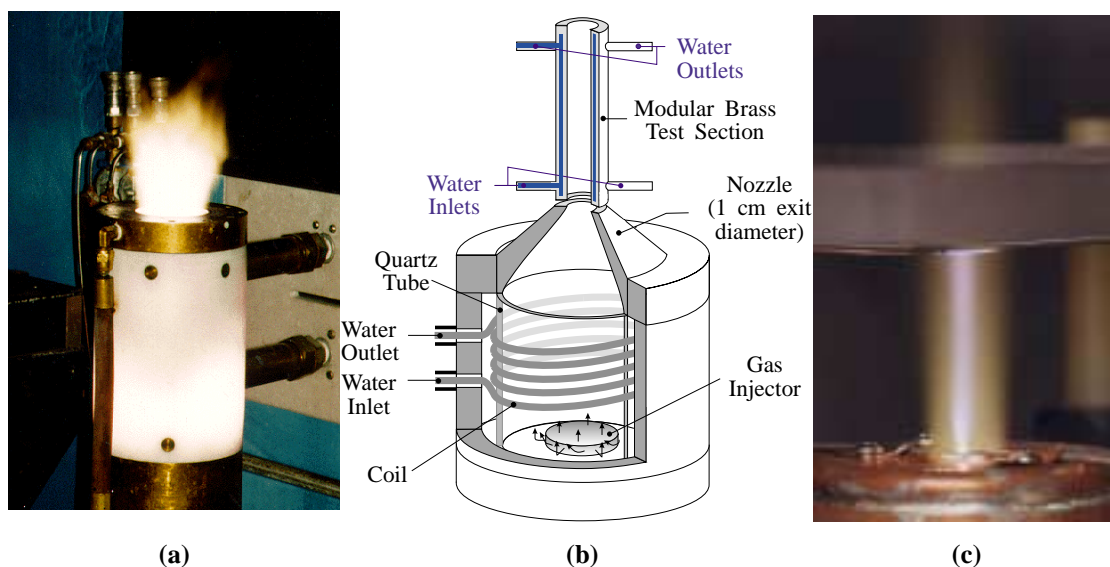


Figure 1. (a) Torch head and plasma plume for LTE air plasma experiments. (b) Schematic of torch head with nonequilibrium test-section for air and nitrogen recombination experiments. (c) DC glow discharge experiments in air at 2200 K (1.4 kV/cm, 200 mA). Interelectrode distance = 3.5 cm. The measured electron number density in the bright discharge region is approximately 10^{12} cm $^{-3}$.

Figure 2 shows a schematic of the experimental set-up for optical emission spectroscopy measurements. All OES measurements presented here were made with a SPEX 750 M monochromator fitted with a 2000x800 pixel SPEX CCD camera. Absolute calibrations of the measured spectral intensities were made using radiance standards including a calibrated tungsten strip lamp and a 1 kW calibrated argon arc. Spherical mirrors and/or MgF2 lenses were employed in the optical train to minimize chromatic aberrations in the ultraviolet, and various long-pass filters were employed to reduce second and higher order light.

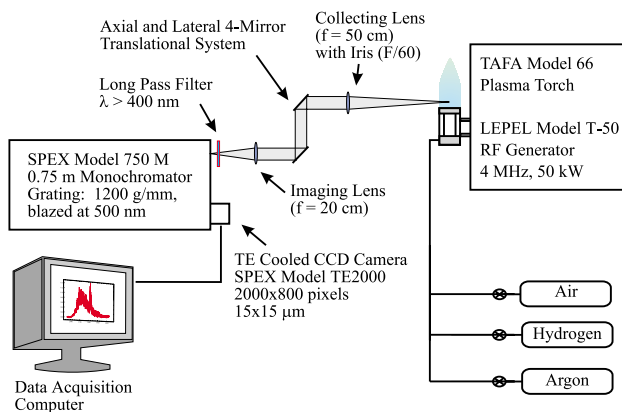


Figure 2. Typical experimental set-up for emission diagnostics.

3 Spectroscopic Model

Considerable work has been devoted in our laboratory to the development of spectroscopic models for the interpretation of air plasma diagnostics. The NEQAIR2 code [1, 5] was built on the basis of the NonEquilibrium Air Radiation code (NEQAIR) of Park [6]. The current version of NEQAIR2 [5] models 27 molecular transitions between electronic states of NO, N₂, N₂⁺, O₂, CN, OH, NH, and CO for a total of several million rotational lines and several hundred of atomic lines of N, O, and C. The model provides accurate simulations of the absolute spectral emission and absorption of air from 180 nm to 5.5 micron. As an illustration of the capabilities of the model, Figure 3 shows a comparison between *absolute* intensity emission spectra measured in LTE air at a temperature approaching 8000 K and NEQAIR2 predictions. As can be seen from the figure, the model closely reproduces the intensity and spectral position of the experimental spectra.

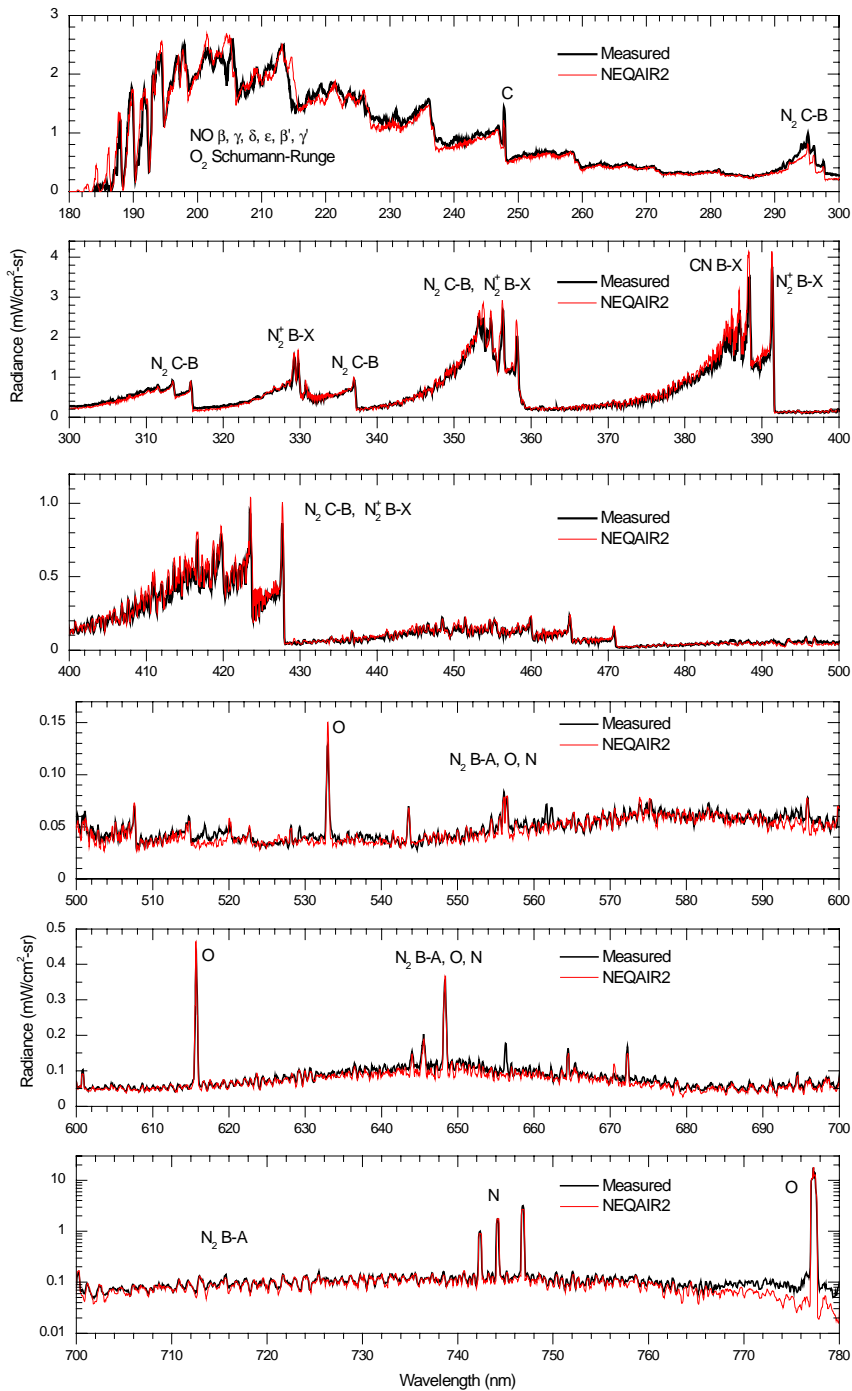


Figure 3. Comparison between NEQAIR2 and measured spectrum of LTE air at ~8000 K.

4 Temperature Measurements

In LTE plasmas, a single temperature characterizes all internal energy modes (vibrational, rotation, electronic). This temperature can be determined from the absolute intensity of any atomic or molecular features, or from Boltzmann plots of vibrational or rotational population distributions. Figure 4 shows temperature profiles measured in the LTE air plasma of Figure 1a. All spectroscopic measurements were Abel-inverted to produce radial temperature profiles [1]. The LTE and Boltzmann temperatures are based on the absolute and relative intensities, respectively, of various atomic lines. The rotational temperature profiles were obtained from measurements of the NO γ (0–1) band shape, using the technique proposed by Gomès et al. [7]. The measured rotational temperature profile is to within experimental uncertainty in agreement with the electronic temperatures. The vibrational temperature profile was measured from the relative intensities of the (0–0) and (2–1) bandheads of N_2^+ (first negative system) at 391.4 nm and 356.4 nm, respectively. The measured vibrational temperatures

have an average uncertainty of ~8%. As can be seen from Figure 4, the measured vibrational, rotational, and electronic temperature profiles are to within experimental uncertainty in good agreement with each other.

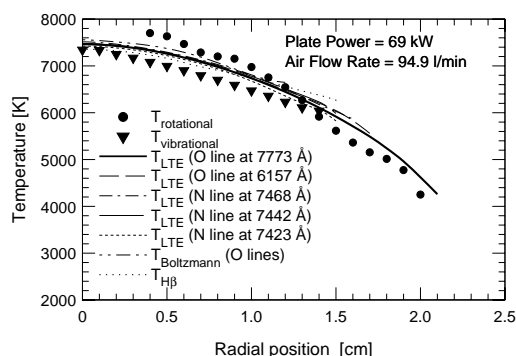


Figure 4. Measured electronic, vibrational, and rotational temperature profiles in LTE air.

In nonequilibrium plasmas, several of the techniques described in the foregoing paragraph may not provide reliable information about the gas temperature because of departures from equilibrium in the distribution of internal energy state populations. The gas temperature is then best inferred from the intensity distribution of rotational lines. Various transitions can be used, depending on the level of plasma excitation. In low temperature humid air plasmas, the emission spectrum of the OH A-X transition around 300 nm provides a particularly useful thermometer. At higher temperatures, or in the presence of an electric field, the OH transition is overlapped by strong emission from N₂ C-B (second positive system). In this case, the rotational temperature can be measured from N₂ C-B rotational lines. At even higher temperatures or higher electric field excitation, many molecular transitions appear in the spectrum and an accurate spectroscopic model is required to extract individual lines of a particular system. For these conditions, we recently proposed a method based on rotational lines of N₂⁺ B-X [8]. The OH, N₂, and N₂⁺ rotational temperature measurement techniques are described in the following subsections.

4.1 OH A-X rotational temperature measurements

The OH A-X transition is one of most intense systems emitted by low temperature air plasmas containing even a small amounts (~1%) of H₂ or H₂O. The rotational temperature can be obtained by fitting the entire band, or more simply from the relative intensities of two groups of rotational lines corresponding to the R and P branches of the (0-0) vibrational band. These branches form distinct peaks at 306.8 and 309.2 nm, respectively, as shown in Figure 5. The spectroscopic model used in NEQAIR2 for OH A-X is described in Ref. [9]. As can be seen from Figure 5, the relative intensity of the two peaks is fairly sensitive to the rotational temperature. Another advantage of the technique is that it does not require absolute or relative intensity calibration because the response of usual detection systems is nearly constant over the less than 3 nm spectral range of interest. This OH transition was used to measure rotational temperatures in our recombination experiments at temperatures below 4000 K [2], and also in our glow experiments (Figure 1c) without the discharge applied [10]. The OH spectrum measured in the glow experiments without discharge applied is shown in Figure 6. The best fit temperature is 2200 ± 50 K.

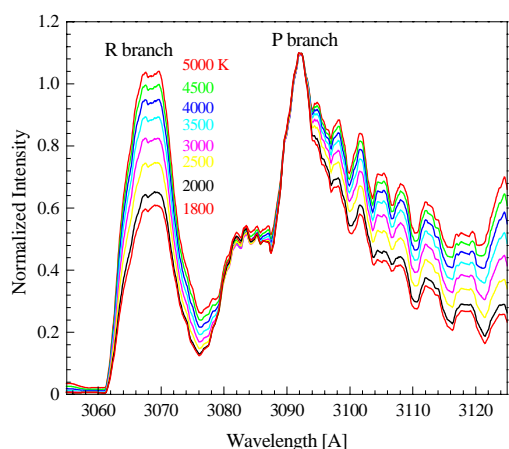


Figure 5. NEQAIR2 simulations of OH A-X (0-0) emission normalized to P branch peak,

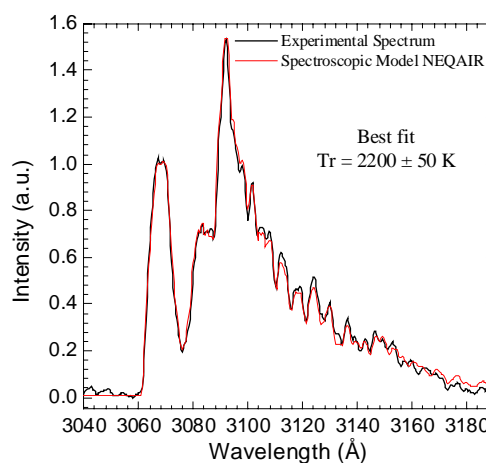


Figure 6. Experimental spectrum measured for the conditions of Figure 1c with no electric field applied,

as a function of the rotational temperature.

and best fit NEQAIR2 spectrum.

4.2 N₂ C-B rotational temperature measurements

At higher temperatures or higher plasma excitation such as for the conditions of Figure 1c with the electrical discharge applied, the OH emission spectrum becomes obscured by other emission systems. Under these conditions, the rotational temperature can be measured from the N₂ C-B (second positive) or NO A-X (gamma) transitions. An example of NO gamma rotational temperature measurement in high temperature LTE air was already described in the introduction of this Section. The use of the N₂ C-B transition is illustrated in Figure 7. The latter spectrum was obtained in the glow experiments of Fig. 1c, with the discharge applied. The best fit NEQAIR2 spectrum yields a temperature of 2200 ± 50 K, which is very close to the temperature without the discharge applied.

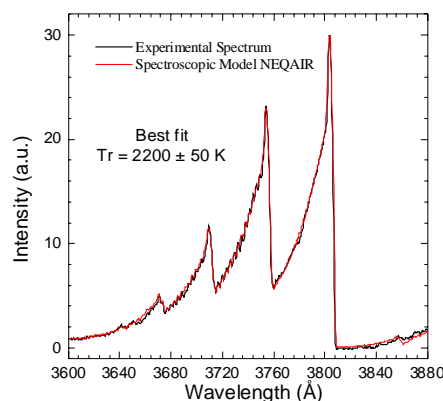


Figure 7. Measured N₂ C-B spectrum in the atmospheric pressure air glow discharge (conditions of Figure 1c). NEQAIR2 best fit provides a rotational temperature of 2200 ± 50 K.

4.3 N₂⁺ B-X rotational temperature measurements

At yet higher excitation levels, the NO gamma and N₂ second positive systems increasingly suffer from overlap by transitions from NO Rydberg states (NO delta, epsilon), O₂ Schumann-Runge, CN violet, and N₂⁺ first negative. The N₂⁺ first negative system (B-X transition) can be used to measure the rotational temperature, provided that an accurate spectroscopic model is available to extract N₂⁺ lines from the encroaching lines of CN and N₂ that emit in the same spectral range. The modeling is complicated by perturbations that affect the positions, intensities, and splitting of the N₂⁺ lines. Recent spectroscopic analyses by Michaud et al. [11] have provided accurate spectroscopic constants that were incorporated in NEQAIR2. This technique was successfully applied to rotational temperature measurements in a recombining nitrogen/argon plasma at the exit of a 15 cm test-section (Figure 1b). The rotational temperature was measured to be 4850 ± 100 K [8], an accuracy far superior to that of other N₂⁺ rotational temperature measurement techniques (see review by Scott et al. [12] for instance).

5 Species Concentration Measurements

5.1 Ground state atomic species concentrations

It is often thought that emission spectroscopy only allows the determination of excited state concentrations. For ground state concentration measurements, one usually resorts to other diagnostics such as absorption, LIF, or other laser based techniques. We will discuss in this section an emission spectroscopy technique that allows the measurement of absolute ground state species concentrations. This technique was first proposed by Laux [1] for the measurement of ground state populations of nitrogen and oxygen atoms. The basic idea is that predissociating molecular electronic states tend to be in equilibrium with the predissociation products, and that this partial equilibrium provides a direct measurement of the concentrations of predissociation products. The technique is of particular interest if the predissociation products are ground state atoms. Two predissociating molecular states of importance in air are the C state of NO (upper state of the C-X or delta transition), and the $v=13$ level of the N₂ B state (upper state of the B-A or first positive system).

Measurements of ground state N and O concentrations from NO delta emission:

In the emitting $C^2\Pi$ state of the NO delta transition, all rovibrational levels above $v=0$ and $J>4.5$ undergo predissociation because of an interference with the $a^4\Pi$ state of NO (see for example Ref. [13]). As shown in Ref. [1], the dominant terms in the rate equation controlling the population of a given predissociating rovibrational level (v, J) of the C state are the rate of predissociation and the rate of repopulation of this level by inverse predissociation. Inverse predissociation is a collisional process by which ground state N (4S) and O (3P) atoms approach along the NO $a^4\Pi$ potential curve, which crosses the potential curve of the $C^2\Pi$ state, and form NO in state (C,v,J). Accordingly, the rate equation for the population of state (C,v,J) is well approximated by:

$$d[\text{NO}_{C,v,J}]/dt \cong -k_{pred} [\text{NO}_{C,v,J}] + k_{inv.pred} [\text{N}] [\text{O}] \quad (1)$$

where k_{pred} and $k_{inv.pred}$ stand for the rate coefficients of predissociation and inverse predissociation, respectively and the square brackets denote species concentrations. Under steady-state conditions, Equation (1) becomes:

$$k_{pred} [\text{NO}_{C,v,J}] \cong k_{inv.pred} [\text{N}] [\text{O}] \quad (2)$$

Equation (2) expresses a very important condition, namely that the *predissociated levels of the C state of NO are in partial equilibrium with ground state oxygen and nitrogen atoms*. Equation 2 can be expressed in a slightly different form by considering the law of mass action for the predissociation reaction:

$$k_{pred} [\text{NO}_{C,v,J}]^{eq} = k_{inv.pred} [\text{N}]^{eq} [\text{O}]^{eq}, \quad (3)$$

where superscript *eq* denote LTE concentrations, and by dividing Equation (2) by Equation (3). We obtain:

$$[\text{NO}_{C,v,J}] / [\text{NO}_{C,v,J}]^{eq} \cong [\text{N}] / [\text{N}]^{eq} \times [\text{O}] / [\text{O}]^{eq} \quad (4)$$

which can be written in compact form as:

$$\rho_{\text{NO}(C,v,J)} \cong \rho_{\text{N}} \times \rho_{\text{O}} \quad (5)$$

In the final Equation (5), the quantity ρ_s , defined as $\rho_s \equiv [s]/[s]^{eq}$, stands for the *nonequilibrium population factor* of species s . Equation (5) shows how nonequilibrium populations of atomic oxygen and nitrogen affect the population of NO C,v,J via predissociation coupling. If N and O atoms are overpopulated with respect to equilibrium by factors of 10 and 100, respectively, then the NO C,v,J states are overpopulated by a factor of 1000 relative to LTE. Such a situation may occur in recombining plasmas where atomic species remain overpopulated with respect to equilibrium as a result of finite recombination rates—see for instance Gessman et al. [2]. On the other hand, if the plasma is close to LTE the concentrations of atomic oxygen and nitrogen are equal to their equilibrium values, and therefore the C state population is also in equilibrium.

This powerful technique is illustrated here with measurements made in a flowing plasma of 10% air-90% argon forced to recombine from a temperature of 7900 K to 3450 K within 750 μs [2, 14]. Initially the dissociation fractions of nitrogen and oxygen are about 98.3 and 99.9%, respectively. Under chemical equilibrium conditions at 3450 K, the dissociation fraction of oxygen molecules is still very high, about 89%, but the dissociation fraction of nitrogen molecules is less than 0.07%. Due to finite recombination rates, nitrogen atoms do not reach equilibrium and thus a significant overpopulation of N atoms may exist in the plasma. The overpopulation factor of the NO C state is given by $\rho_{\text{NO}(C,v,J)} \cong \rho_{\text{N}}$ (ρ_{O} is very close to one because the equilibrium concentration of O atoms does not change appreciably from 7900 to 3450 K). If the gas temperature can be measured separately, the factor $\rho_{\text{NO}(C,v,J)}$ is inferred by taking the ratio of the measured absolute emission spectrum of NO C-X to the predicted LTE NO C-X spectrum at the measured temperature. The nitrogen atom concentration is then directly obtained by multiplying the equilibrium concentration of N atoms at the measured temperature by the overpopulation factor of nitrogen atoms.

Measurements of ground state N concentrations from N₂ B-A emission

The technique of ground state atomic concentration measurements can be further illustrated with the predissociating B state of N₂. In contrast with the C state of NO, for which most rovibrational levels predissociate, the B state of N₂ is mainly predissociated around vibrational level $v=13$. The population of $v=13$ is controlled by predissociation and inverse predissociation of ground state nitrogen atoms, but also by vibrational relaxation and other collisional processes. A detailed study of the various kinetic processes controlling the population of the vibrational levels of the B state of N₂ was conducted using a collisional-radiative model of nitrogen plasmas developed in our laboratory [15, 16]. This model comprises 337 vibronic states of N₂ and N₂⁺ and 23 electronic states of N and N⁺. Approximately 11000 reactions between these individual states are taken into account, including electronic and vibrational excitation by electron impact, ionization by electron impact, dissociation by electron and heavy particle impact, VT and VV transfer, charge transfer, dissociative recombination, radiative emission and predissociation. With this model, it was shown that the main processes controlling the population of N₂ (B,v=13) are predissociation and its inverse. It follows that the nonequilibrium population factor of N₂ (B,v=13) can be related to the ground state nonequilibrium population factor of nitrogen atoms by the simple relation:

$$\rho_{N_2(B, v=13)} \equiv \rho_N \times \rho_N$$

This relation can then be used to determine the nitrogen atom population using the procedure illustrated with the following experimental example. This experiment was conducted in a recombining nitrogen plasma (~ 100 slpm N_2), premixed before injection into the torch with ~ 50 slpm of argon. The plasma was rapidly cooled from a temperature of 7200 K to 4850 K within 250 μ s in a 15 cm long water-cooled test section. The experimental set-up was similar to that shown in Figure 1b. The gas temperature of 4850 K was measured separately from rotational lines of the N_2^+ first negative system, as described in Section 4.3 and in Ref. [8]. Absolute emission spectra of the N_2 B-A transition were measured between 5000 and 8000 \AA (see Figure 7). These spectra were compared with a calculated LTE spectrum using the measured gas temperature profile. Fig. 7 shows that the measured spectrum is much more intense than the computed equilibrium spectrum. The observed differences indicate departures from a Boltzmann distribution in the vibrational levels of the N_2 B state. The nonequilibrium vibrational population distribution was inferred by multiplying the equilibrium populations of individual vibrational levels by nonequilibrium factors chosen so as to match the measured spectrum. The measured distribution of nonequilibrium population factors (Fig. 8) is characteristic of the Lewis-Rayleigh afterglow mechanism [17] and peaks around $v=13$. Since the nonequilibrium factors are larger than unity, an excess of nitrogen atoms exist, consistent with the finite rate of nitrogen atom recombination. The overpopulation factor of $v=13$ is measured to be $\rho_{N_2 B, v=13} = 66 \pm 4$. Thus the overpopulation of nitrogen atoms is approximately 8.1 ± 0.3 . At 4850 ± 100 K, the equilibrium concentration of nitrogen atoms in the nitrogen/argon plasma mixture is $2.0 \pm 0.4 \times 10^{16} \text{ cm}^{-3}$. Multiplying this number by the measured overpopulation factor ρ_N , we infer a nonequilibrium nitrogen atom concentration of $1.6 \pm 0.4 \times 10^{17} \text{ cm}^{-3}$. These measurements are in very good agreement with the collisional-radiative model predictions shown in Fig. 9 of the population factors of various electronic states of N_2 . Figure 9 underscores the importance of departures from LTE in nonequilibrium plasmas, even at atmospheric pressure.

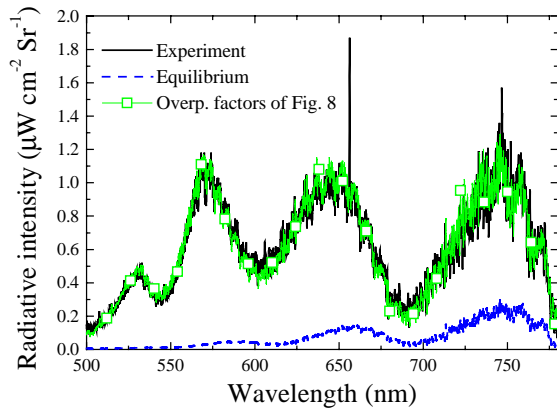


Figure 7. LTE and non-LTE NEQAIR2 spectra vs. spectral measurements in a recombining nitrogen/argon plasma. The non-LTE NEQAIR2 spectrum includes the vibrational overpopulation factors of Fig. 8.

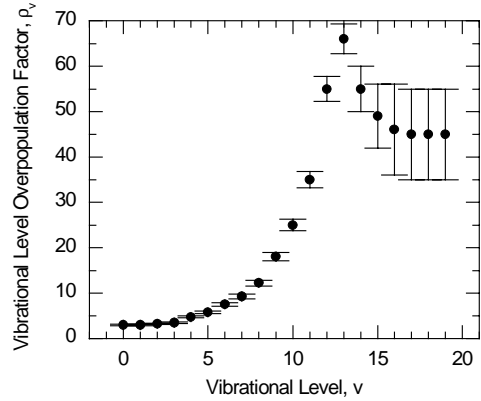


Figure 8. Measured N_2 B state overpopulation factors in the recombining N_2 /Ar plasma.

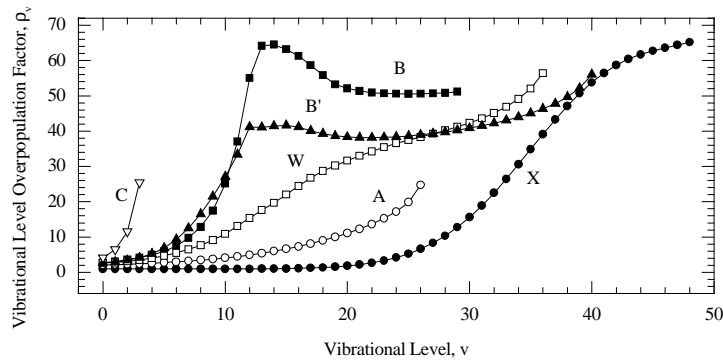


Figure 9. Predicted vibrational overpopulation factors for the N_2 X, A, B, W, B' and C states of N_2 in a recombining nitrogen/argon plasma for the conditions of Figures 7 and 8.

5.2. Electron number densities

In plasmas with electron number densities greater than $\sim 10^{13} \text{ cm}^{-3}$, spatially and temporally-resolved electron number densities can be obtained from the lineshape of the Balmer β transition (4-2) of atomic hydrogen at 486.1 nm. This technique requires the presence of a small amount (typically 1-2% mole fraction) of hydrogen, which may either come from dissociated water vapor in humid air, or from premixing H_2 in the air stream.

The lineshape of the H_β transition is a function of Lorentzian (Stark, van der Waals, resonance, natural) and Gaussian (Doppler) broadening mechanisms that result in a Voigt profile. The Lorentzian half width at half maximum (HWHM) is the sum of the Lorentzian HWHMs. Numerical expressions for the Doppler, van der Waals, resonance, and natural widths of the H_β line in air plasmas were derived in Ref. [1]. They are summarized in Table 1 for conditions of interest in air plasmas with small amounts of hydrogen. The Stark HWHM fit given in Table 1 is based on the NBS tables of Ref. [18] and is valid for electron densities between 10^{13} and 10^{17} cm^{-3} .

Table 1. Half Widths at Half Maximum (in \AA) for the H_β line at 4861.32 \AA . P is the pressure in atm., T the temperature in K, n_e the electron number density in cm^{-3} , and X_H the mole fraction of hydrogen atoms.

$\Delta\lambda_{\text{Stark}}$	$\Delta\lambda_{\text{resonance}}$	$\Delta\lambda_{\text{van der Waals}}$	$\Delta\lambda_{\text{Natural}}$	$\Delta\lambda_{\text{Doppler}}$
$1.74 \times 10^{-10} (n_e)^{0.647}$	$302 X_H (P/T)$	$(24.5 - 6.00 \times 10^{-4})(P/T^{0.7})$	3.1×10^{-4}	$1.74 \times 10^{-3} \sqrt{T}$

This technique was employed in our laboratory to measure electron number densities in air and nitrogen plasmas under various degrees of nonequilibrium [1, 2]. To illustrate the technique, we describe here measurements made in an LTE air plasma [1]. The entrance and exit slits of the $\frac{3}{4}$ meter monochromator were set to 20 μm . The grating has 1200 grooves/mm. The instrumental slit function was approximately trapezoidal, with HWHM of 0.11 \AA . A small amount of H_2 (1.7% mole fraction) was premixed with air before injection into the plasma torch. The spatial resolution of the measurements, determined by the width of the entrance slit and the magnification of the optical train, was approximately 0.13 mm.

A line-of-sight emission spectrum measured along the plasma diameter is shown in Fig. 10. Also shown in Fig. 10 is the “background” spectrum due to the emission of other species present in the plasma. The largest contribution to this background is from the first positive system of N_2 ($\text{B}^3\Pi - \text{A}^3\Sigma$ transition). The background was measured after switching off the hydrogen flow. Without hydrogen, the plasma temperature was measured to be lower by approximately 200 K. The plasma power was slightly readjusted in order to return to the same temperature conditions by matching the intensity of the background spectral features away from the H_β linecenter. Figure 11 shows the H_β lineshape obtained after subtracting the background signal from the total spectrum. The measured lineshape is well fitted with a Voigt profile of HWHM = 1.10 \AA . For these conditions, the HWHMs of the various broadening mechanisms and of the resulting Voigt profile are shown in Fig. 12. The measured HWHM corresponds to an electron number density of $1.4 \times 10^{15} \text{ cm}^{-3}$.

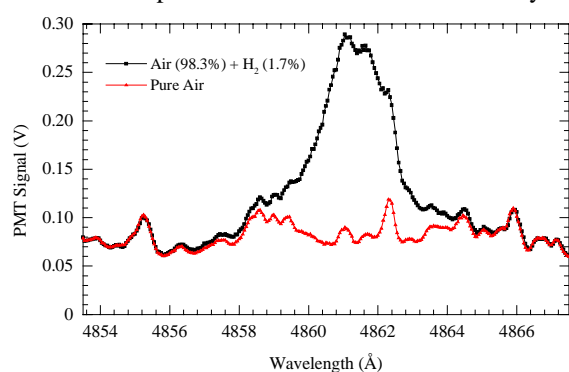


Figure 10. Typical emission scan in the region of H_β line. The underlying emission features are mostly due to the first positive system of N_2 .

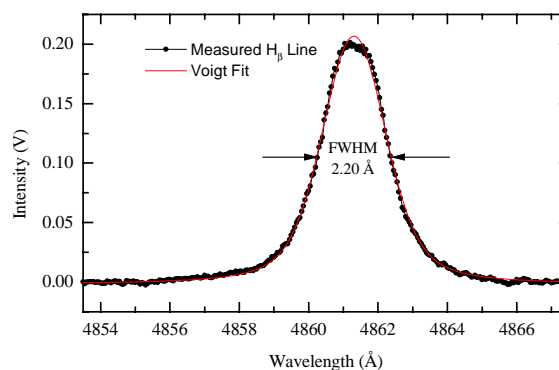


Figure 11. H_β lineshape obtained from the difference of the two signals shown in Fig.10 and Voigt fit.

Of the broadening mechanisms plotted in Fig. 12, only Stark broadening depends explicitly on the electron number density. Doppler, Van der Waals and resonance broadening widths depend on the gas temperature. For LTE plasmas the electron number density is also function of the temperature, as given by the Saha equation. In Figure 12 we have made use of the Saha equilibrium relation between temperature and electron number density to plot all broadening widths as a function of the equilibrium electron number density. In this regard, the Voigt widths shown in Fig. 12 should only be used to determine the electron number density in equilibrium plasmas. In

nonequilibrium plasmas, the Doppler, van der Waals and resonance widths should be replaced with values based on the actual gas temperature, which must then be determined separately. Figure 13 illustrates this case for a gas temperature of 2000 K. At low temperatures van der Waals broadening becomes increasingly significant and is effectively larger than Stark broadening at electron densities smaller than $7 \times 10^{13} \text{ cm}^{-3}$.

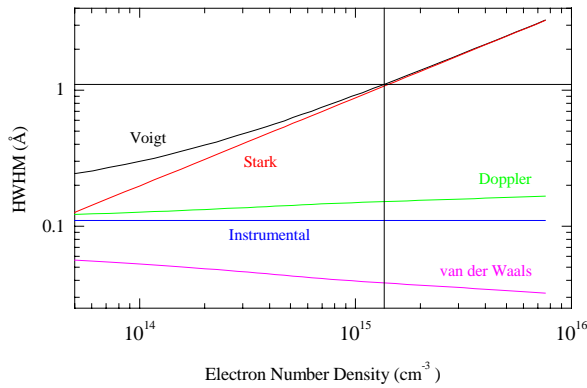


Figure 12. H_{β} lineshape broadening as a function of electron number density in *equilibrium*, atmospheric pressure air. (Instrumental FWHM = 0.11 Å)

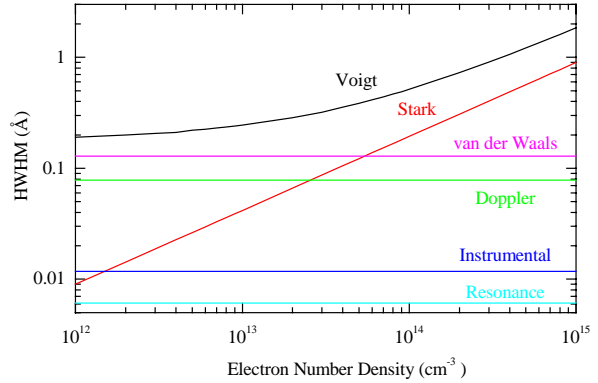


Figure 13. H_{β} lineshape broadening as a function of the electron number density in 2000 K atmospheric pressure air. (Instrumental FWHM = 0.011 Å)

In axisymmetric plasma geometries, local H_{β} line profiles can be obtained by Abel-inverting a set of lateral scans of H_{β} lineshapes. We have used this technique in our experiments with LTE air plasmas [1]. The H_{β} lineshape was scanned at 25 lateral locations along chords of the 5 cm diameter plasma. The electron number density profile determined from the Abel-inverted lineshapes is shown in Fig. 14. The measured profile is found to be in very good agreement with chemical equilibrium electron densities based on an LTE temperature profile measured with the 7773 Å oxygen line.

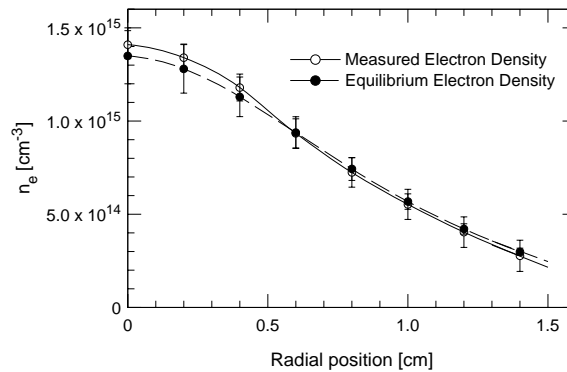


Figure 14. Measured (solid) and equilibrium (dashes) electron number density profiles.

Figure 15 shows another example of H_{β} lineshape measurement in a low temperature air plasma (about 4500 K) with electron number densities approaching 10^{13} cm^{-3} . In this case the H_{β} line intensity was so weak relative to the nitrogen background that the spectra had to be measured in second order to reduce the instrumental FWHM with respect to the other broadening widths. Long CCD averaging times of 10 seconds were employed. The inferred number density of $5 \times 10^{13} \text{ cm}^{-3}$ represents a lower detection limit for this method.

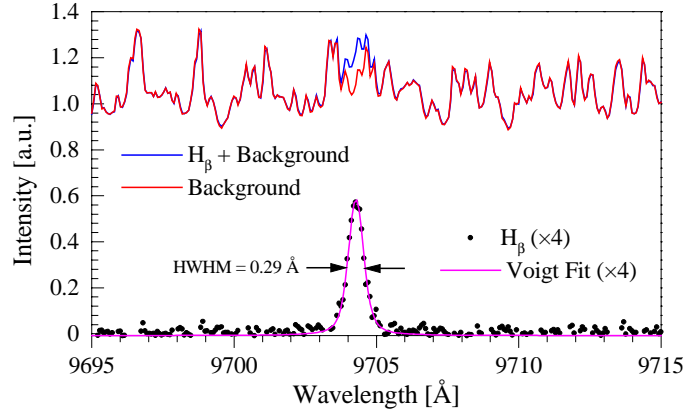


Figure 15. H_{β} lineshape in a low temperature (~ 4500 K) LTE air plasma. Here the H_{β} lineshape was measured in second order so as to reduce instrumental broadening to approximately 0.07 Å.

5.3. Cavity Ring-Down Spectroscopy

Cavity Ring-Down Spectroscopy (CRDS) is a sensitive direct-absorption technique that has been successfully employed in our laboratory to detect dilute concentrations of N_2^+ in atmospheric-pressure air and nitrogen plasmas [19, 20]. N_2^+ tends to be the dominant ion in nitrogen discharges, and thus the N_2^+ measurement enables one of the most direct measurements of electron number density. In air, the concentration of N_2^+ may be linked to that of electrons through charge balance approaches. Because the concentration of N_2^+ (and electrons) is often relatively small (on the order of 1 ppm), a sensitive diagnostic, such as CRDS, is required.

In CRDS, light from a pulsed or continuous-wave laser source is injected into a high-finesse optical cavity (the ring-down cavity) formed by two or more highly reflective mirrors [21, 22]. With the input radiation terminated, light trapped in the ring-down cavity, I_{circ} , decays exponentially with time, t , as:[23]

$$I_{circ}(t) = I_{circ}(t_0) \exp[-(\alpha cl + n(1-R) + L) \times (t - t_0) / T_r],$$

where T_r is the round-trip transit time, R is the mirror reflectivity, α is the absorption cross section of the absorbing species present within the cavity at concentration c , n is the number of mirrors that comprise the ring-down cavity, l is the round-trip pathlength of the ring-down cavity, and L accounts for other losses within the cavity including absorption and scattering by the mirror surfaces. By fitting the ring-down waveform to the function $I_0 \exp[-t/\tau]$, the decay rate, $1/\tau$, may be determined. This decay or “ring-down” rate is simply related to the concentration of absorbing species within the ring-down cavity:

$$1/\tau = (\alpha cl + n(1-R) + L) / T_r.$$

By plotting the decay rate as a function of wavelength, an absorption spectrum of species present within the cavity is generated. If the empty-cavity decay rate, $1/\tau_0$, and absorption cross section of the absorbing species are known, then the absolute concentration of absorbing species is determined from:

$$c = (1/\tau - 1/\tau_0) \times (T_r / \alpha l).$$

The inherent sensitivity of the CRDS technique stems from the insensitivity of the decay rate to fluctuations in the light source intensity, fluctuations that ultimately limit the sensitivity of other direct-absorption techniques. Furthermore, the light pulse traverses the ring-down cavity many times resulting in effective pathlengths that exceed the sample length by thousands of times.

Figure 16 shows a schematic of one of our CRDS experiments [19]. A tunable Nd:YAG pumped dye or optical parametric oscillator (OPO) laser system and a two-mirror ring-down cavity are used to probe the rotationally resolved absorption spectrum of N_2^+ (B \leftarrow X) around 390 nm. Pulses of light from the laser system are mode matched to the ring-down cavity using beam shaping optics. The light exiting the cavity is detected with a fast photomultiplier tube (PMT). Current generated by the photomultiplier is digitized using a digitizing oscilloscope, and a computer is then used to fit the decay waveforms to an exponential function and extract $1/\tau$, while scanning the laser through a wavelength range of interest. In order to obtain spatially resolved measurements, the ring-down cavity is translated across the plasma discharge (or vice versa). The technique has excellent spatial resolution (on the order of a few beam waists), and we are currently exploring techniques to improve the temporal resolution [20].

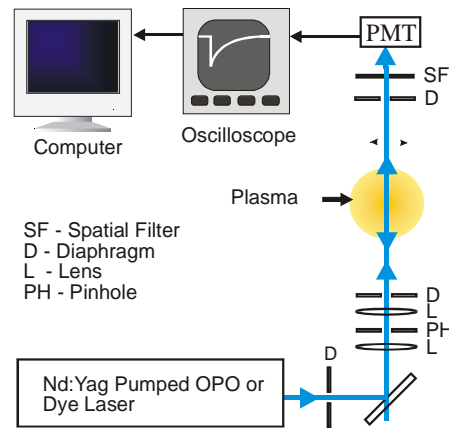


Figure 16. Schematic diagram of CRDS setup used to probe N_2^+ .

Figure 17 shows the absorption spectrum of N_2^+ near the (0-0) bandhead, as measured with the CRDS technique in an LTE air plasma, as well as the absorption spectrum predicted by NEQAIR2. The width of the absorption feature generated by NEQAIR2 was broadened to fit the width of the observed absorption feature. After broadening, the intensity of the predicted transition is in excellent agreement with that obtained experimentally. The temperature of the air plasma, determined independently via emission spectroscopy, was approximately 7000 K. Each spectral element represents an average of 10 decay rates, each obtained by fitting a waveform that was itself an average of 25 single-shot waveforms.

A spatial profile of the concentration of N_2^+ was obtained by measuring the absorption by N_2^+ at 391.6 nm as the ring-down cavity was translated from the center to the edge of the plasma at 0.2 cm intervals with a spatial resolution of 0.5 mm. An Abel transform was employed to extract N_2^+ absorption as a function of radial distance from the center of the plasma. Using the absorption cross section obtained from NEQAIR2, the absolute concentration of N_2^+ was obtained as a function of radial distance (see Figure 18). These N_2^+ concentrations are in excellent agreement with the LTE N_2^+ concentrations calculated from the plasma temperature profile, which was obtained by measuring the integrated absolute intensity of the O triplet at 777.3 nm.

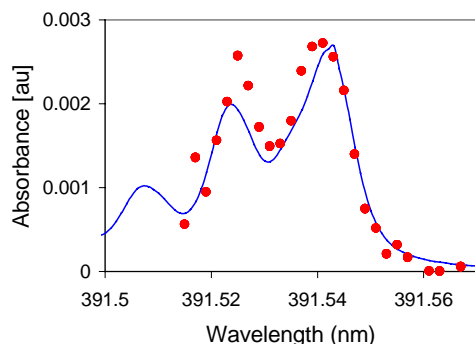


Figure 17. Experimental (points) and simulated (line) absorption spectrum of the N_2^+ bandhead in LTE air plasma at 7000 K.

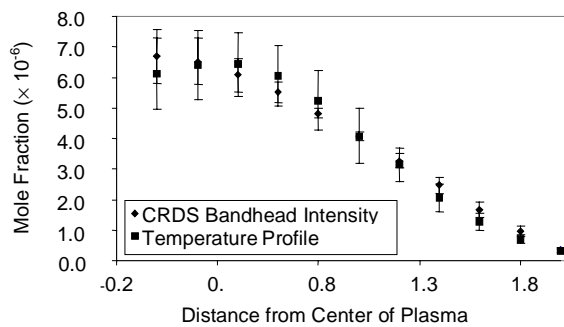


Figure 18. Concentration profile of N_2^+ obtained by Abel inversion of absorbance profile and LTE calculation using LTE temperature profile.

6 Conclusion

Several optical techniques have been presented that can be used to measure rotational temperatures and the concentrations of neutral and charged species in air and nitrogen plasmas. These techniques typically offer high (submillimeter) spatial resolution. We are currently interested in applying these diagnostics with high temporal resolution on the order of nano and microseconds. These high temporal diagnostics are motivated by the study of a new class of repetitively pulsed discharges in atmospheric pressure air. We have recently proposed these discharges as a way to generate atmospheric pressure air plasmas with power requirements two to three orders of magnitude lower than for DC discharges [4]. In these discharges, a short (1–10 ns) high-voltage pulse is used to generate free electrons, which subsequently recombine over about 10 microseconds, after which time another pulse is provided. Conventional CRDS assumes that the absorptive losses are uniform over the duration of the ring-down signal, so that a single exponential decay time characterizes the ring-down, and the absorption. In

principle, for a time varying case, one may fit different exponential decays to different temporal windows within the ring-down. Then, each decay time represents the losses in the corresponding temporal interval, and from a single ringdown one can obtain multiple absorption measurements. With such an approach, the temporal resolution is limited to the roundtrip transit time of the light within the cavity (order 5 ns). Alternatively, one may think that the temporal resolution of conventional CRDS is given by the ringdown time itself (order 5 μ s). We are currently investigating temporally resolved approaches as a means of measuring the peak electron concentration (at the end of the high voltage pulse), as well as the electron concentration during the recombination period between pulses.

Acknowledgements

The authors wish to acknowledge Richard Gessman, Denis Packan, Lan Yu, Laurent Pierrot, Thomas Owano, Thomas Spence, and Azer Yalin for their contributions to the work presented in this paper. This work was funded by the Director of Defense Research & Engineering (DDR&E) within the Air Plasma Ramparts MURI Program managed by the Air Force Office of Scientific Research.

References

- [1] C.O. Laux, "Optical Diagnostics and Radiative Emission of Air Plasmas," PhD. Thesis, *Mechanical Engineering Department*, Stanford University, Stanford, CA (1993).
- [2] R.J. Gessman, C.O. Laux, and C.H. Kruger, "Experimental study of kinetic mechanisms of recombining atmospheric pressure air plasmas," AIAA Paper 97-2364, 28th AIAA Plasmadynamics and Lasers Conference, Atlanta, GA (1997).
- [3] C.O. Laux, R.J. Gessman, D.M. Packan, L. Yu, C.H. Kruger, and R.N. Zare, "Experimental Investigations of Ionizational Nonequilibrium in Atmospheric Pressure Air Plasmas," 25th IEEE International Conference on Plasma Science (ICOPS), Raleigh, NC (1998).
- [4] M. Nagulapally, G.V. Candler, C.O. Laux, L. Yu, D.M. Packan, C.H. Kruger, R. Stark, and K.H. Schoenbach, "Experiments and Simulations of DC and Pulsed Discharges in Air Plasmas," AIAA Paper 2000-2417, 31st AIAA Plasmadynamics and Lasers Conference, Denver, CO (2000).
- [5] C.O. Laux, R.J. Gessman, and C.H. Kruger, "Measurements and Modeling of the Absolute Spectral Emission of Air Plasmas between 185 and 800 nm," JQSRT (to be submitted 2001).
- [6] C. Park, "Nonequilibrium Air Radiation (NEQAIR) Program: User's Manual," NASA-Ames Research Center, Moffett Field, CA, Technical Memorandum TM86707 (1985).
- [7] A.M. Gomès, J. Bacri, J.P. Sarrette, and J. Salon, *J. Analytical Atomic Spectroscopy* **7** (1992) 1103-9.
- [8] C.O. Laux, R.J. Gessman, C.H. Kruger, F. Roux, F. Michaud, S.P. Davis, *JQSRT* **68** (2001) 473-82.
- [9] D.A. Levin, C.O. Laux, and C.H. Kruger, *JQSRT* **61** (1999) 377-392.
- [10] C.O. Laux, L. Yu, D.M. Packan, R.J. Gessman, L. Pierrot, C.H. Kruger, and R.N. Zare, "Ionization Mechanisms in Two-Temperature Air Plasmas," AIAA Paper 99-3476, 30th AIAA Plasmadynamics and Lasers Conference, Norfolk, VA, 1999.
- [11] F. Michaud, F. Roux, S.P. Davis, A.-D. Nguyen, and C.O. Laux, *J. Molec. Spectrosc.* **203** (2000) 1-8.
- [12] C.D. Scott, H.E. Blackwell, S. Arepalli, M.A. Akundi, *J. Thermophys. Heat Transfer* **12** (1998) 457-64.
- [13] G.E. Gadd, D.L. Huestis, and T.G. Slanger, *Journal of Chemical Physics* **95** (1991) 3944.
- [14] R.J. Gessman, "An Experimental Investigation of the Effects of Chemical and Ionizational Nonequilibrium in Recombining Air Plasmas," Ph.D. Thesis, Mechanical Engineering Dept., Stanford University, Stanford, CA (2000).
- [15] L. Pierrot, C.O. Laux, and C.H. Kruger, "Vibrationally-Specific Collisional-Radiative Model for Nonequilibrium Nitrogen Plasmas," AIAA Paper 98-2664, 29th AIAA Plasmadynamics and Lasers Conference, Albuquerque, NM (1998).
- [16] L. Pierrot, L. Yu, R.J. Gessman, C.O. Laux, and C.H. Kruger, "Collisional-radiative modeling of nonequilibrium effects in nitrogen plasmas," AIAA Paper 99-3478, 30th AIAA Plasmadynamics and Lasers Conference, Norfolk, VA (1999).
- [17] H. Partridge, S.R. Langhoff, and C.W. Bauschlicher, *Journal of Chemical Physics* **88** (1988) 3174-86.
- [18] C.R. Vidal, J. Cooper, and E.W. Smith, *The Astrophysical Journal Supplement Series* **25** (1973) 37-136.
- [19] T.G. Spence, J. Xie, R.N. Zare, D.M. Packan, L. Yu, C.O. Laux, T.G. Owano, C.H. Kruger, and R.N. Zare, "Cavity Ring-Down Spectroscopy Measurements of N_2^+ in Atmospheric Pressure Air Plasmas," AIAA Paper 99-3433, 30th AIAA Plasmadynamics and Lasers Conference, Norfolk, VA, 1999.

- [20] A.P. Yalin, U.Lommatzsch, R.N. Zare, C.O. Laux, and C.H. Kruger, "Cavity Ring-Down Spectroscopy of N_2^+ in Pulsed and DC Atmospheric Pressure Discharges," to be presented at International Conference on Plasma Science, Las Vegas, NV (June 2001).
- [21] A. O'Keefe and D.A.G. Deacon, *Review of Scientific Instruments* **59** (1988) 2544-51.
- [22] P. Zalicki and R.N. Zare, *Journal of Chemical Physics* **102** (1995) 2708-17.
- [23] A.E. Siegman, *Lasers*. Mill Valley: University Science Books (1986).